An Approximate Solution in Spectral Domain for Plane Wave Scattering by a Thick Half-Plane

Mayumi NAKAGAWA [1], Hironori FUJII [1] and Kazunori UCHIDA [1]
[1] *Fukuoka Institute of Technology*
3-30-1 Wajiro-Higashi, Higashi-ku Fukuoka, 811-0295 JAPAN
k-uchida@fit.ac.jp

Abstract

In this paper we attempt to derive simplified spectral expressions for plane-wave scattering from a half-plate by investigating the analytical behavior of the rigorous Wiener-Hopf (WH) solutions numerically. We show how the WH solutions depend on the incident angle and thickness of the half-plate, and we compare the proposed approximate solutions with the WH solutions to check the accuracy of the approximate expressions. It is shown numerically that the proposed solutions are in good agreement with the WH solutions when the incident angle is chosen as $\theta > 90°$.

1. Introduction

The two-dimensional (2D) plane wave scattering by a thick conducting half-plate is one of the fundamental electromagnetic field problems. It includes the influence of reflection from the faces of the half-plate as well as diffraction at the wedges of it. This problem can be solved rigorously in spectral domain by applying the WH technique [1]-[3] to the 2D wave equation. To obtain the WH solutions in space domain, however, we need to calculate its Fourier inverse transformations.

When the half-plane is thin, the scattered field can be expressed analytically both in spectral and space domains [1]-[3]. When it is thick, however, the spectral functions of the scattered fields should be solved in terms of infinite simultaneous equations [4]. Moreover, their Fourier inverse transformations cannot be performed analytically. In this context, the rigorous WH solutions are too complicated for us to apply them to practical electromagnetic problems such as propagation in urban areas. As a result, we attempt to derive a simple expression for the same problem by considering the analytical properties of the WH solutions numerically.

In this paper, we deal with the case of E-wave incidence focusing on the far fields. In Sec. 2, we first show the rigorous solutions in spectral domain obtained by applying the WH technique to the present problem. We investigate numerically the analytical properties of the WH solutions focusing on the effect of the incident angle and the thickness of the half-plate. It is shown that these properties are well approximated by a sampling function in case of $\theta > 90°$. Therefore, we can derive an approximate expression in spectral domain as shown in Sec.3.

In order to check the accuracy of the introduced simple expression, we compare the numerical results of the present method with the WH solutions in Sec.4. According to the numerical examples, it is shown that the results of the simple expression are in good agreement with the WH solutions in spectral domain under the condition $\theta > 90°$.

2. Wiener-Hopf solutions

Fig.1 shows the geometry of the 2D plane wave scattering by a conducting half-plate. The thickness of the half-plate is $2b$ and the incident angle of the plane-wave (E-wave) is $\theta(0 < \theta < \pi)$.

Now, we define the total(t), incident(i) and scattered(s) fields as follows:

$$(\boldsymbol{E}^t, \boldsymbol{H}^t) = (\boldsymbol{E}^i, \boldsymbol{H}^i) + (\boldsymbol{E}^s, \boldsymbol{H}^s) \tag{1}$$

where the leading function of incident wave (E-wave) is expressed as follows:

$$E_z^i = e^{-j\kappa x\cos\theta - j\kappa y\sin\theta}, \tag{2}$$

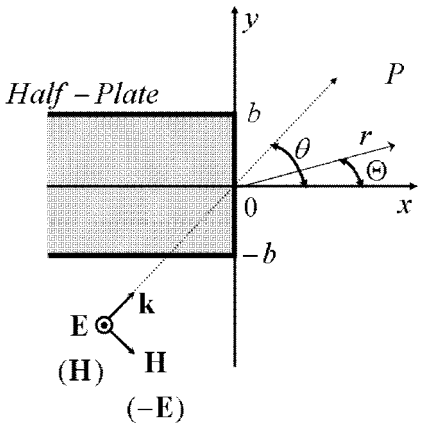

Fig. 1: Geometry of the problem for a half-plate.

and the Maxwell equations are rewritten as follows:

$$(\frac{\partial^2}{\partial x^2}+\frac{\partial^2}{\partial y^2}+\kappa^2)E_z^s(x,y)=0 \tag{3}$$

$$H_x^s=\frac{-1}{j\omega\mu_0}\cdot\frac{\partial E_z^s}{\partial y} \tag{4}$$

$$H_y^s=\frac{1}{j\omega\mu_0}\cdot\frac{\partial E_z^s}{\partial x} \tag{5}$$

where the time dependence $e^{j\omega t}$ is assumed and the wave number in the free space is expressed as follows:

$$\kappa=\omega\sqrt{\epsilon_0\mu_0}. \tag{6}$$

In order to obtain the spectral function of the scattered field based on the WH technique, we use the following Fourier transformation pair defined by

$$\begin{aligned}F(\zeta)&=\int_{-\infty}^{\infty}f(x)e^{j\zeta x}dx\\ f(x)&=\frac{1}{2\pi}\int_c F(\zeta)e^{-j\zeta x}d\zeta\end{aligned} \tag{7}$$

where the contour "c" is in the common domain "D" of the upper "U" and lower "L" half-planes as shown in Fig.2. These domain are constituted by assuming a small loss in the free space.

The rigorous solutions of scattered field in spectral domain can be obtained by applying the WH technique after calculating the complex Fourier transformation of the wave equation as follows:

$$\begin{aligned}E_z^s(\zeta,y)&=\frac{je^{-jk(y-b)}}{2G_c^+(\zeta)}\cdot\frac{U_c^+(\zeta_\theta)G_c^+(\zeta_\theta)}{(\zeta-\zeta_\theta)}\\ &+\frac{je^{-jk(y-b)}}{2G_c^+(\zeta)}\sum_{n=1}^{\infty}\frac{U_c^+(-k_{cn})b_{cn}^2G_c^-(k_{cn})}{(k_{cn}+\zeta_\theta)(\zeta-k_{cn})k_{cn}}\\ &+\frac{je^{-jk(y-b)}}{2G_s^+(\zeta)}\cdot\frac{U_s^+(\zeta_\theta)G_s^+(\zeta_\theta)}{(\zeta-\zeta_\theta)}\\ &+\frac{je^{-jk(y-b)}}{2G_s^+(\zeta)}\sum_{n=1}^{\infty}\frac{U_s^+(-k_{sn})b_{sn}^2G_s^-(k_{sn})}{(k_{sn}+\zeta_\theta)(\zeta-k_{sn})k_{sn}}\\ &=\Lambda_p(\zeta)\frac{j\sqrt{\kappa-\zeta_\theta}}{(\zeta-\zeta_\theta)\sqrt{\kappa-\zeta}}e^{-jk(y-b)}\\ &+\Omega_p(\zeta)\frac{j\sqrt{\kappa}}{\sqrt{\kappa-\zeta}}e^{-jk(y-b)}\end{aligned} \tag{8}$$

$(y>b)$

$$\begin{aligned}E_z^s(\zeta,y)&=\frac{je^{jk(y+b)}}{2G_c^+(\zeta)}\cdot\frac{U_c^+(\zeta_\theta)G_c^+(\zeta_\theta)}{(\zeta-\zeta_\theta)}\\ &+\frac{je^{jk(y+b)}}{2G_c^+(\zeta)}\sum_{n=1}^{\infty}\frac{U_c^+(-k_{cn})b_{cn}^2G_c^-(k_{cn})}{(k_{cn}+\zeta_\theta)(\zeta-k_{cn})k_{cn}}\\ &-\frac{je^{jk(y+b)}}{2G_s^+(\zeta)}\cdot\frac{U_s^+(\zeta_\theta)G_s^+(\zeta_\theta)}{(\zeta-\zeta_\theta)}\\ &-\frac{je^{jk(y+b)}}{2G_s^+(\zeta)}\sum_{n=1}^{\infty}\frac{U_s^+(-k_{sn})b_{sn}^2G_s^-(k_{sn})}{(k_{sn}+\zeta_\theta)(\zeta-k_{sn})k_{sn}}\\ &=\Lambda_m(\zeta)\frac{j\sqrt{\kappa-\zeta_\theta}}{(\zeta-\zeta_\theta)\sqrt{\kappa-\zeta}}e^{jk(y+b)}\\ &+\Omega_m(\zeta)\frac{j\sqrt{\kappa}}{\sqrt{\kappa-\zeta}}e^{jk(y+b)}\end{aligned} \tag{9}$$

$(y<-b)$

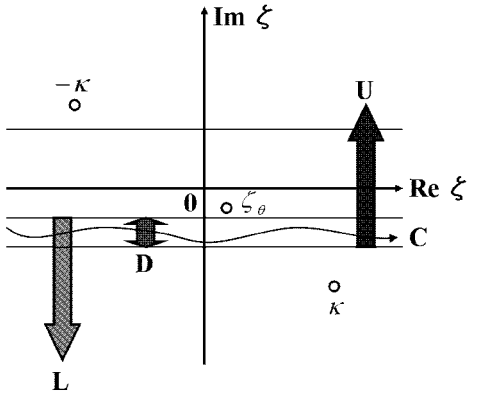

Fig. 2: Contour c in the common domain D in the ζ-plane.

where, we omit the calculation of the scattered field in the $-b<y<b$ because discussions are restricted only to the far-field.

In Eqs.(8) and (9), we rearrange the spectral expressions into two parts depending on whether it includes the infinite simultaneous equations or not. They are defined by use of $\Lambda_{p,m}(\zeta)$ and $\Omega_{p,m}(\zeta)$ as follows:

$$\begin{aligned}\Lambda_{p,m}(\zeta)=\Big[&\frac{\sqrt{\kappa-\zeta}}{G_c^+(\zeta)}\cdot\frac{G_c^+(\zeta_\theta)}{\sqrt{\kappa-\zeta_\theta}}\cdot\frac{U_c^+(\zeta_\theta)}{2}\\ &\pm\frac{\sqrt{\kappa-\zeta}}{G_s^+(\zeta)}\cdot\frac{G_s^+(\zeta_\theta)}{\sqrt{\kappa-\zeta_\theta}}\cdot\frac{U_s^+(\zeta_\theta)}{2}\Big],\end{aligned} \tag{10}$$

$$\Omega_{p,m}(\zeta) = \left[\frac{\sqrt{\kappa-\zeta}}{2\sqrt{\kappa}G_c^+(\zeta)} \times \sum_{n=1}^{\infty} \frac{U_c^+(-k_{cn})b_{cn}^2 G_c^-(k_{cn})}{(k_{cn}+\zeta_\theta)(\zeta-k_{cn})k_{cn}} \pm \frac{\sqrt{\kappa-\zeta}}{2\sqrt{\kappa}G_s^+(\zeta)} \times \sum_{n=1}^{\infty} \frac{U_s^+(-k_{sn})b_{sn}^2 G_s^-(k_{sn})}{(k_{sn}+\zeta_\theta)(\zeta-k_{sn})k_{sn}} \right] \tag{11}$$

where the upper script "+" denotes regularity of the spectral function in upper half-plane "U", the upper scripts c and s correspond to even and odd components of the unknown spectral functions.

The pole of the spectral function is given by $\zeta_\theta = \kappa\cos\theta$, and the residues of the unknown spectral functions at the pole $\zeta = \zeta_\theta$ are given in relation to the incidet wave as follows:

$$U_c^+(\zeta_\theta) = 2\cos(k_\theta b) \tag{12}$$

$$U_s^+(\zeta_\theta) = -2j\sin(k_\theta b) \tag{13}$$

$$k_\theta = \sqrt{\kappa^2-\zeta_\theta^2}. \tag{14}$$

The coefficients of $U_{c,s}^+(\zeta)$ at $(\zeta = -k_{qm})$ are determined by the following infinite simultaneous equations:

$$U_q^+(-k_{qm}) = U_q^+(\zeta_\theta)\frac{G_q^+(\zeta_\theta)}{G_q^+(-k_{qm})} + \frac{(k_{qm}+\zeta_\theta)}{G_q^+(-k_{qm})} \times \sum_{n=1}^{\infty} \frac{U_q^+(-k_{qn})b_{qn}^2 G_q^-(k_{qn})}{(k_{qn}+\zeta_\theta)(k_{qm}+k_{qn})k_{qn}} \quad (q=c,s, m=1,2,3,\cdots). \tag{15}$$

The kernel functions $G_c(\zeta)$ and $G_s(\zeta)$ and their factorized functions are defined as follows [5]:

$$G_c(\zeta) = G_q^+(\zeta)G_q^+(-\zeta) = \frac{jkb}{\cos kb}e^{jkb}, \quad G_s(\zeta) = G_q^+(\zeta)G_q^+(-\zeta) = \frac{kb}{\sin kb}e^{jkb} \quad (q=c,s) \tag{16}$$

where

$$k = \sqrt{\kappa^2-\zeta^2}, \quad b_{cn} = (n-1/2)\pi/b, \quad b_{sn} = n\pi/b, \quad k_{cn}^2 = \kappa^2 - b_{cn}^2, \quad k_{sn}^2 = \kappa^2 - b_{sn}^2. \tag{17}$$

Fourier inverse transformation of the spectral function leads to the scattered field in the space domain as follows:

$$E_z^s(x,y) = \frac{1}{2\pi}\int_c E_z^s(\zeta,y)e^{-j\zeta x}d\zeta. \tag{18}$$

In particular, when the thickness of half-plate is zero (thin half-plane), we have the following famous analytical solution in spectral domain:

$$E_z^s(\zeta,y) = \frac{j\sqrt{\kappa-\zeta_\theta}}{(\zeta-\zeta_\theta)\sqrt{\kappa-\zeta}}e^{-jk|y|} \tag{19}$$

where, $-\pi < \Theta < \pi$ and we have assumed the following change of variables between cartesian expression is defined by [2]:

$$x = r\cos\Theta, y = r\sin\Theta. \tag{20}$$

Fourier inverse transform in Eq.(19) can be calculated as follows:

$$E_z^s(x,y) = -e^{-j\kappa r\cos(\Theta-\theta)} \times F[-\sqrt{2\kappa r}\sin\frac{1}{2}(\Theta-\theta)] - e^{-j\kappa r\cos(\Theta+\theta)} \times F[\sqrt{2\kappa r}\sin\frac{1}{2}(\Theta+\theta)] = \Psi(r,\theta,\Theta), (-\pi<\Theta<\pi). \tag{21}$$

The following Fresnel functions are used in the above solution Eq.(21), and are define by:

$$F(X) = \begin{cases} \frac{e^{\frac{\pi}{4}j}}{\sqrt{\pi}}\int_X^\infty e^{-ju^2}du & (X>0) \\ 1 - \frac{e^{\frac{\pi}{4}j}}{\sqrt{\pi}}\int_{-X}^\infty e^{-ju^2}du. & (X<0) \end{cases} \tag{22}$$

Next, we investigate the analytical properties of the functions $\Lambda_{p,m}(\zeta)$ and $\Omega_{p,m}(\zeta)$ to introduce their approximate solutions in a simplified form. Figs.3 and 4, show the behavior of $\Lambda_p(\zeta)$ and $\Omega_p(\zeta)$ at $\zeta[-\kappa, \kappa]$ in case of $\theta <= 90^\circ$ and $\theta > 90^\circ$. Figs.5 and 6 show the behavior of these functions where the thickness of the half-plate is chosen as a parameter. Other parameters are selected as $f = 300MHz$ and $\theta = 30^\circ$ and 150°.

According to these numerical results, we can summarize the analytical properties in the following form. First, we describe the behavior of $\Lambda_{p,m}(\zeta)$ as follows:

1) $\Lambda_{p,m}(\zeta)$ is characterized by the incident angles $\theta <= 90^\circ$ and $\theta > 90^\circ$.
2) $\Lambda_{p,m}(\zeta)$ is independent on the thickness of the half-plate.
3) Amplitude of $\Lambda_{p,m}(\zeta)$ is maximum at $\zeta/\kappa \simeq 0.2$.

Second, we describe the behavior of $\Omega_{p,m}(\zeta)$ as follows:

1) $\Omega_{p,m}(\zeta)$ is also characterized by the incident angles $\theta <= 90^\circ$ and $\theta > 90^\circ$.
2) In the case of $\theta <= 90^\circ$, the amplitude of $\Omega_{p,m}(\zeta)$ is maximum at $\zeta/\kappa \simeq 0.2$, and there is little dependence on the thickness of a half-plate.
3) In the case of $\theta > 90^\circ$, as the incident angle increases, the amplitude of $\Omega_{p,m}(\zeta)$ is increased at ζ/κ.

4) The maximum amplitude of $\Omega_{p,m}(\zeta)$ increases along with the thickness of a half-plate, but the width of $\Omega_{p,m}(\zeta)$ is narrow.
5) $\Omega_{p,m}(\zeta)$ is analogous to a sampling function.

Now, based on the above survey of $\Omega_{p,m}(\zeta)$ and $\Lambda_{p,m}(\zeta)$, we introduce simple spectral expressions so as to solve Fourier inverse transformation easily. In case of $\theta > 90°$, as mentioned above, $\Omega_{p,m}(\zeta)$ exhibits strongly the reflection and diffraction caused by the thickness of the half-plane. It seems possible to introduce a simple expression for $\Omega_{p,m}(\zeta)$ involving infinite simultaneous equations.

3. APROXIMATION

As shown in Sec.2, the functions $\Lambda_{p,m}(\zeta)$ and $\Omega_{p,m}(\zeta)$ defined by Eqs.(10) and (11) exhibit complicated behaviors depending on the incident angle θ and the thickness b of the half-plane. However, since the function $\Omega_{p,m}(\zeta)$ resembles to to a sampling function in case of $\theta > 90°$, we can approximate the above functions as follows:

$$\Lambda_{p,m}(\zeta) \simeq \Lambda_{p,m}(\zeta_\theta) = e^{\mp jk_\theta b} \tag{23}$$

$$\Omega_{p,m}(\zeta) \simeq \frac{\kappa \sin(\zeta \mp \zeta_\theta) b}{2(\zeta \mp \zeta_\theta)}. \tag{24}$$

As a result, the spectral functions of the scattered field given in Eqs.(8) and (9) can be approximated as follows:

$$\begin{aligned} E_z^s(\zeta, y) \simeq\ & e^{-jk_\theta b} \frac{j\sqrt{\kappa - \zeta_\theta}}{(\zeta - \zeta_\theta)\sqrt{\kappa - \zeta}} e^{-jk(y-b)} \\ & + \frac{\kappa \sin(\zeta - \zeta_\theta) b}{2(\zeta - \zeta_\theta)} \frac{j\sqrt{\kappa}}{\sqrt{\kappa - \zeta}} e^{-jk(y-b)}, \\ & (y > b) \end{aligned} \tag{25}$$

$$\begin{aligned} E_z^s(\zeta, y) \simeq\ & e^{jk_\theta b} \frac{j\sqrt{\kappa - \zeta_\theta}}{(\zeta - \zeta_\theta)\sqrt{\kappa - \zeta}} e^{jk(y+b)} \\ & + \frac{\kappa \sin(\zeta + \zeta_\theta) b}{2(\zeta + \zeta_\theta)} \frac{j\sqrt{\kappa}}{\sqrt{\kappa - \zeta}} e^{jk(y+b)}. \\ & (y < -b) \end{aligned} \tag{26}$$

Now we carry out the Fourier inverse transformation of the above equations obtain the scattered field in space domain; we use the Fresnel function for the first terms in Eqs.(24) and (25), and we apply the saddle point method to the second terms [6]. Then, an approximate expression for the scattered field in space domain is given by

$$\begin{aligned} E_z^s(x, y) \simeq\ & e^{-j\kappa b \sin\theta} \Psi(r_1, \theta, \Theta_1) \\ & + \frac{\sqrt{2}\kappa}{2} \frac{\sin[(\cos\Theta_1 + \cos(\pi - \theta))\kappa b]}{(\cos\Theta_1 + \cos(\pi - \theta))} \\ & \times \cos(\frac{\Theta_1}{2}) \Phi(r) \\ & (y > b, \quad \theta > \frac{\pi}{2}) \end{aligned} \tag{27}$$

$$\begin{aligned} E_z^s(x, y) \simeq\ & e^{-j\kappa b \sin\theta} \Psi(r_1, \theta, \Theta_1) \\ & + \frac{\sqrt{2}\kappa}{2} \frac{\sin[(|\cos\Theta_1| + |\cos(\pi - \theta)|)\kappa b]}{(|\cos\Theta_1| + |\cos(\pi - \theta)|)} \\ & \times \cos(\frac{\Theta_1}{2}) \Phi(r) \\ & (y > b, \quad \theta < \frac{\pi}{2}) \end{aligned} \tag{28}$$

$$\begin{aligned} E_z^s(x, y) \simeq\ & e^{+j\kappa b \sin\theta} \Psi(r_2, \theta, \Theta_2) \\ & + j\frac{\sqrt{2}\kappa}{2} \frac{\sin[(|\cos\Theta_2| + |\cos(\pi - \theta)|)\kappa b]}{(|\cos\Theta_2| + |\cos(\pi - \theta)|)} \\ & \times \cos(\frac{\Theta_2}{2}) \Phi(r) \\ & (y < -b) \end{aligned} \tag{29}$$

where the following polar coordinates are assumed

$$\begin{aligned} & r_1 = \frac{x}{\cos\Theta_1}, \quad r_2 = \frac{x}{\cos\Theta_2} \\ & \Theta_1 = \cos^{-1}\frac{\zeta_{\Theta_1}}{\kappa}, \quad \Theta_2 = \cos^{-1}\frac{\zeta_{\Theta_2}}{\kappa}. \end{aligned} \tag{30}$$

4. NUMERICAL EXAMPLES

We show some numerical results of the present method in comparison with the WH solutions in order to check the accuracy of the simple expressions. Figs.7 and 8 show the amplitudes of the scattered far fields in case of $\theta > 90°$. In these numerical examples, parameters are chosen as the incident angle is $\theta = 120°$ and $145°$, and thickness of the half-plate is $b = 10.1\lambda$ and 30.1λ. When the incident angle is $\theta = 145°$, the approximate solutions are in good agreement with the WH solutions, even if the thickness of the half-plate is changed from $b = 10.1\lambda$ to $b = 30.1\lambda$. However, when the incident angle is $\theta = 120°$, the amplitude of the main lobe of the present method is much larger than the WH solution, although the width of the main lobes are in good agreement. This property is also shown for another incident angles in case of $\theta > 90°$.

5. CONCLUSION

In this paper we have dealt with the plane wave scattering by a thick half-plane, and we have attempted to introduce an approximate solution in a simple form by rearranging the rigorous spectral function obtained by the WH technique. Approximations have been made in the spectral domain, and the Fourier inverse transformations have been performed analytically. In case of $\theta > 90°$, it is shown that the function $\Omega_p(\zeta)$, that includes infinite simultaneous equation, can be approximated by a sampling function. The numerical results of the approximate solution have been compared with the WH solutions.

According to the numerical examples, the approximate solutions are in good agreement with the WH solutions in case of $\theta > 90°$. In other cases, however, satisfactory agreements were not obtained. To overcome this disagreement is to deserve as a future problem.

ACKNOWLEDGMENTS

The work was supported in part by a Grand-in Aid for Scientific Research (C) (17560354) from Japan Society for the Promotion of Science.

REFERENCES

[1] D.S.Jones, "Diffraction by thick semi-infinite plate", *Proc. R. Soc.*, A217, 1953, p. 153.

[2] B. Noble, "Methods based on the Wiener-Hopf technique", *Programon Press*, 1958.

[3] K. Mittra and S. Lee, "Analytical techniques in the theory of guided waves", *The Macmillan Co.*, 1978, pp. 113.

[4] M. NAKAGAWA ,H. FUJII and K. UCHIDA, "On accuracy of ray tracing method solution for scattering problem by thick half-plane", *EMT-05-69.*, 2005, pp. 49-54 (in Japanese).

[5] K. Uchida and K. Aoki, "Factorization procedure for Wiener-Hopf kernels", *Bulletin of Engineering at Kyushu Uni.*, vol.52, no.2, 1979, pp. 141-147.

[6] K. Uchida ,H. Maeda, T.Imai, T. Fujii and M. Hata, "Analysis of electromagnetic wave scattering by a conducting thin plate and image coefficient for ray tracing method", *IEICE Trans. Electron.*, vol.E81-C, no.6, 1998, pp. 993-999.

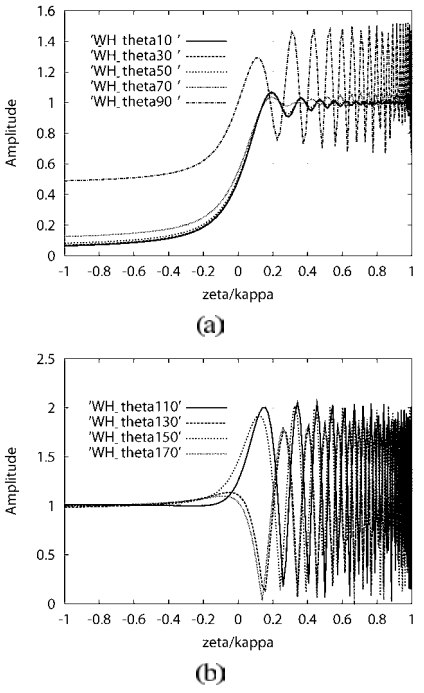

Fig. 3: The characteristic of $\Lambda_p(\zeta)$ depend on the incident angle (a)$\theta <= 90°$($\theta = 10°, 30°, 50°, 70°$ and $90°$), (b)$\theta > 90°$($\theta = 110°, 130°, 150°$ and $170°$) (WH solutions).

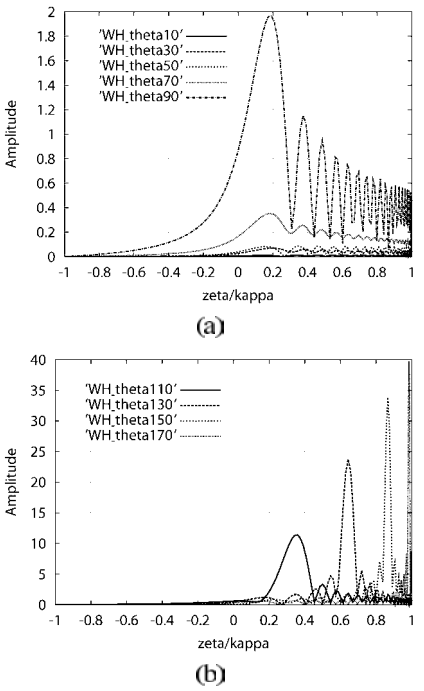

Fig. 4: The characteristic of $\Omega_p(\zeta)$ depend on the incident angle (a)$\theta <= 90°$($\theta = 10°, 30°, 50°, 70°$ and $90°$), (b)$\theta > 90°$($\theta = 110°, 130°, 150°$ and $170°$) (WH solutions).

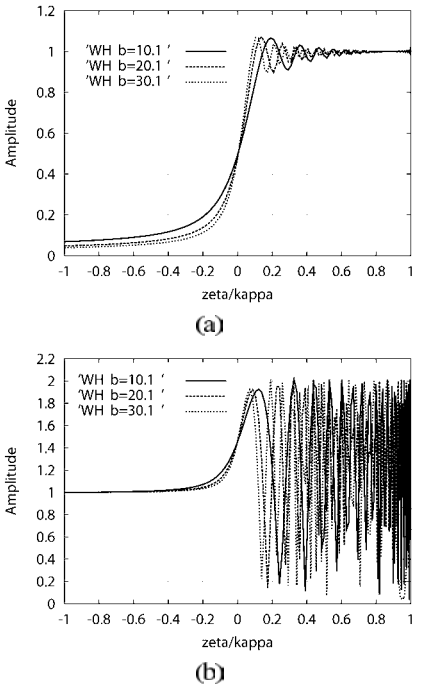

Fig. 5: The characteristic of $\Lambda_p(\zeta)$ depend on the thickness of the half-plate($b = 10.1, 20.1$ and 30.1λ) for (a)$\theta = 30°$, (b)$\theta = 150°$(WH solutions).

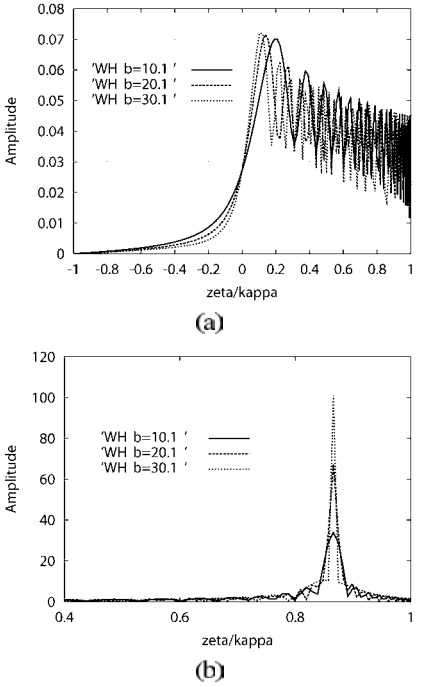

Fig. 6: The characteristic of $\Omega_p(\zeta)$ depend on the thickness of the half-plate($b = 10.1, 20.1$ and 30.1λ) for (a)$\theta = 30°$, (b)$\theta = 150°$(WH solutions).

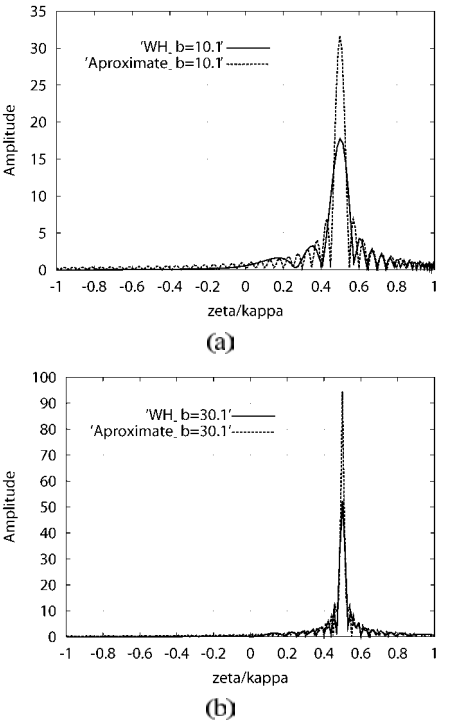

Fig. 7: Comparison WH solutions with approximate solutions for $\theta = 120°$, (a)$b = 10.1\lambda$, (b)$b = 30.1\lambda$.

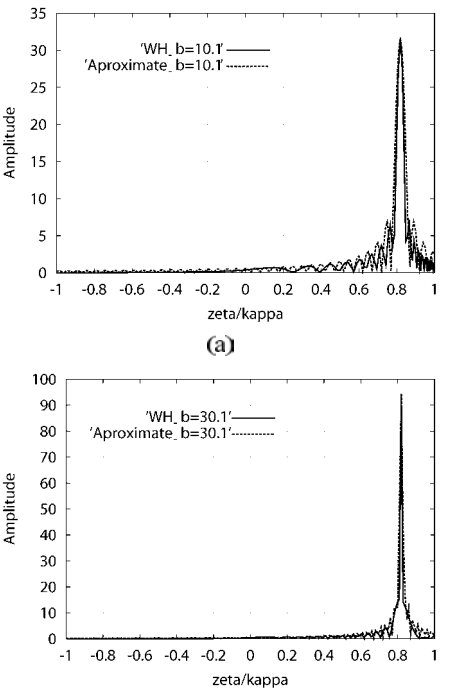

Fig. 8: Comparison WH solutions with approximate solutions for $\theta = 145°$, (a)$b = 10.1\lambda$, (b)$b = 30.1\lambda$.